Available online at www.sciencedirect.com
ScienceDirect
Trans. Nonferrous Met. Soc. China 34(2024) 1110−1122
Transactions of Nonferrous Metals Society of China
www.tnmsc.cn

Effect of solutes on texture evolution during grain growth in ZK60 alloy by phase field simulation

Yu-hao SONG, Ming-tao WANG, Jun-yuan BAI, Jian-feng JIN, Pei-jun YANG, Ya-ping ZONG, Gao-wu QIN

Key Laboratory for Anisotropy and Texture of Materials (MoE), School of Materials Science and Engineering,
Northeastern University, Shenyang 110819, China

Received 7 October 2022; accepted 16 May 2023

Abstract: A three-dimensional (3D) multiscale phase field model was proposed to investigate the effect of Ca, Y and Al solutes on the texture evolution of ZK60 alloy during grain growth at 573 K under an applied compression stress of 270 MPa, in which the characteristics of the elastic anisotropy and grain boundary (GB) segregation caused by the solutes were taken into account. The results show that either Ca or Y addition can weaken the basal texture of ZK60, while Al addition enhances it. The deviation of the grain size distribution from the Hillert model becomes greater with the addition of Al, while Ca or Y addition reduces the deviation. The solute segregation-induced GB energy change has a very limited effect on the texture evolution compared with elastic anisotropy. The revealed mechanism is of great significance for the microstructure design of the ZK60 alloy by an appropriate alloying strategy.

Key words: phase field model; elastic anisotropy; solute segregation; texture evolution; ZK60 alloy; alloying

---

1 Introduction

Magnesium (Mg) alloys have been widely used in many fields because of their light weight, high specific strength, stiffness and easy recycling [1−3]. However, the plastic deformation ability of Mg alloys has been reduced by a strong basal texture which is easily formed during thermo-mechanical processing owing to the intrinsic closed-packed hexagonal (HCP) structure with fewer slip systems. Thus, the formability of Mg alloys [4,5] can be significantly improved by weakening the basal texture according to previous research results. ZK60 alloy is a commonly used commercial wrought Mg alloy, and many experimental studies are trying to weaken the texture to improve its formability and mechanical properties [6−8]. At present, alloying strategy has been proved to be an effective way to solve this problem, and the underlying mechanism has aroused extensive academic interest.

Different alloying elements (solutes) have individual effects on the texture evolution of Mg alloys. Some elements, such as Al, can strengthen the basal texture of wrought Mg alloys [9,10]. Rare earth elements, such as Y, can effectively inhibit the coarsening of basal oriented grains in Mg alloys, and rare-earth addition has become a common method to weaken the processing texture [11−13]. In addition to Y, many studies have indicated that Ca can weaken the basal texture effectively [14], which provides a cheaper alternative for micro-structure improvement. However, researchers have different views on the reasons why these elements weaken the basal texture. LIU et al [15] speculated that the addition of Ca or rare earth elements influenced the texture indirectly by changing the axial ratio (*c*/*a*) of the matrix and stacking fault energy. ZHAO et al [16] attributed the weakening of texture to the combination of the preferential appearance of compression twins and the decrease

---

Corresponding author: Ming-tao WANG, Tel: +86-13904040599, E-mail: wangmingtao@mail.neu.edu.cn

DOI: 10.1016/S1003-6326(23)66457-X

in the axial ratio. In contrast, DING et al [13,17] proposed a weak relation between the axial ratio and the basal texture formation owing to the very limited change in the axial ratio. Based on the results above, although researchers had different viewpoints, they all noted that the change in the crystal axis ratio caused by alloying elements may be one of the reasons for the change in texture. The change in the axial ratio will change the elastic anisotropy of the alloy, leading to a distribution change in the elastic strain energy. Many simulations [18−20] and experiments [21,22] have confirmed that the elastic strain energy plays an important role in microstructure evolution. Therefore, whether solutes affect the microstructure evolution by changing the elastic anisotropy and how various alloying element effects differ need to be further clarified.

Phase field model is an effective computational method in simulations of crystal materials. The combination of simulation methods at different scales can avoid the limitations of different methods well, which makes multiscale simulation a development direction. In this way, XIN et al [23] reported a spinodal strengthened ultralightweight Mg. The phase field model is good at dealing with the material behavior at the microscopic to mesoscopic scale. By relating the phase field to classical density functional theory, the phase field crystal model can simulate the evolution of liquid pools at the atomic scale [24]. Because it is easy to track the interface and the response of the structure to applied fields such as stress and electromagnetism [25], the phase field method can be used to study various phase transition processes [26,27]. Since the formation of texture in alloys is the response of grains with different orientations to the applied stress at elevated temperatures, the phase field modeling is usually an effective way to simulate this process [28−30]. In our previous work, a phase field model was used to study the effect of grain boundary (GB) property anisotropy in ZK60 [31]. However, few studies have been focused on the effects of both the elastic energy of the alloyed matrix and GB property anisotropy when phase field modeling was performed [32,33]. Interestingly, SHAHNOOSHI et al [34] performed a 2D phase field simulation of an elastically deformed polycrystalline microstructure considering the GB property anisotropy and concluded that the GB energy distribution would affect the texture. Unfortunately, they suggested the essential aspect of 3D phase field simulation of stressed grain growth but did not perform it.

In this study, a 3D multiscale phase field model was proposed to investigate the effect of Ca, Y and Al solution atoms on the texture evolution of ZK60 alloy during grain growth at 573 K under a compression stress of 270 MPa. The elastic anisotropy and GB segregation induced by the solutes were taken into account by transferring the significant model parameters obtained from simulation methods at different scales, including first principles and molecular dynamics simulations. In particular, the solutes, Al, Y and Ca, were considered since they were very effective alloying elements to improve the mechanical properties of Mg alloys.

2 Models

2.1 Phase field model

In this model, the evolution of grains can be described by solving the time-dependent Ginzburg−Landau equation [35] as shown below:

$$\frac{\partial \eta_p(\boldsymbol{r},t)}{\partial t} = -L\frac{\delta F}{\delta \eta_p\left(\boldsymbol{r},t\right)},\ p=1,\ 2,\ 3,\ \cdots,\ n \tag{1}$$

where L is a variable related to the grain coarse mobility and can be expressed in the form of the Arrhenius law $L=L_0\exp[-Q/(RT)]$, L_0 can be determined by experimental results calibrated in ZK60 alloy and Q is the thermal activity energy related to GB movement. Finally, the calculated value of L in ZK60 alloy at 573 K is 16.8×10^{-3} mol/(J·s) according to our previous work [36]. F is the function of free energy, η stands for a special orientation by giving a special Euler angle, t is the time, $\boldsymbol{r}$ is the position vector, p is the orientation, and n is the number of grain orientations and can represent an infinite number of arbitrary grain orientations in a real microstructure by adopting the APT algorithm [37,38].

According to previous experiments [39,40], the addition of Ca or Y showed a significant texture-randomizing effect during microstructure evolution when there were few second phase particles. Therefore, this work mainly focused on the influence of the anisotropy of elastic energy and

GB properties on microstructure evolution without considering the second phase particles. Both the elastic energy and orientation-dependent GB energy were coupled in the phase field model. The free energy F can be expressed as follows:

$$F=F_{\mathrm{ch}}+E_{\mathrm{el}} \tag{2}$$

where F_{ch} is the chemical free energy and GB energy is a part of it, and E_{el} is the elastic strain energy. F_{ch} can be expressed as follows:

$$F_{\mathrm{ch}} = \int_V f(\eta_1,\ \eta_2,\ \ldots,\ \eta_p,\ \nabla\eta_1,\ \nabla\eta_2,\ \ldots,\ \nabla\eta_p)\mathrm{d}V = \int_V mf_0\left(\eta_1,\ \eta_2,\ \ldots,\ \eta_p\right)+\frac{K_2}{2}\sum_{i=1}^{p}(\nabla\eta_i)^2]\mathrm{d}V \tag{3}$$

$$f_0 = A-\frac{B_2}{2}\sum_{q=1}^{n}\eta_q^2(\boldsymbol{r},t)+\frac{B_2}{4}\sum_{q=1}^{n}\eta_q^4(\boldsymbol{r},t)+\frac{K_1}{2}\sum_{q=1}^{n}\sum_{p\neq q}^{n}\eta_q^2(\boldsymbol{r},t)\eta_p^2(\boldsymbol{r},t) \tag{4}$$

The GB energy can be expressed by the parameters in F_{ch} according to the previous work [31]. K_1 is coupling item coefficient between two adjacent grains with different orientations, represented by p and q; K_2 and m are related with grain boundary features. Inside a grain, $\frac{K_2}{2}\sum_{i=1}^{p}(\nabla\eta_i)^2=0$, $\frac{K_1}{2}\sum_{q=1}^{n}\sum_{p\neq q}^{n}\eta_q^2(\boldsymbol{r},t)\eta_p^2(\boldsymbol{r},t)=0$ and m is a constant with a value of 1. f_0 is the free energy of ZK60 and can be obtained by CALPHAD-based tools. THERMOCALC is used in this work to calculate the free energy. The related parameters A and B_2 in the free energy function were taken as A=−21.6 kJ/mol and B_2=51.2 J/mol according to our previous work [36], and based on these values, we can determine the values of other model parameters on a real spatial-time scale. In the GB area, $m(\theta)$ and $K_2(\theta)$ are coefficients related to GB energy determined by the dihedral angle θ [31]. Referring to previous work for a homogeneous ZK60 alloy system at 573 K, we took m=1, K_1=2.05×10^2 J/mol and K_2=4.4×10^{-12} J·m^2/mol [31]. Considering that the alloying elements studied in this work would affect the GB energy, the GB energy with alloying was estimated by a stable low-angle tilt grain boundary (TGB) obtained from the MD method and K_2 and m should be modified as

$$K_2(\theta)=K_2^0(\theta)+K_2^{\mathrm{ele}}(\theta) \tag{5a}$$

$$m(\theta)=m^0(\theta)+m^{\mathrm{ele}}(\theta) \tag{5b}$$

where K_2^{ele} and m^{ele} represent the change caused by segregation, which can be obtained from the MD method results and is equal to 0 in ZK60 alloy. K_2^0 and m^0 represent the phase field parameter values in ZK60 alloy system. When the dihedral angle of the GB between adjacent grains is less than 20°, K_2 and m of low-angle grain boundaries can be expressed as follows [31]:

$$K_2^0(\theta)=9.200\times10^{-12}\theta\frac{\pi}{180}\cdot\left[0.317-\ln\left(\theta\frac{\pi}{180}\right)\right] \tag{6a}$$

$$m^0(\theta)=2.093\theta\frac{\pi}{180}\left[0.317-\ln\left(\theta\frac{\pi}{180}\right)\right] \tag{6b}$$

In this way, a database with orientation-dependent GB energy was established according to the orientation number in the model.

Based on the linear elasticity theory introduced by KHACHATURYAN [41], the elastic energy (E_{el}) of a homogeneous anisotropic system can be expressed as

$$E_{\mathrm{el}}=\int_V\frac{1}{2}C_{ijkl}(\boldsymbol{r})\varepsilon_{kl}(\boldsymbol{r})\varepsilon_{ij}(\boldsymbol{r})\mathrm{d}V \tag{7}$$

where V is the volume, $\varepsilon_{ij}(\boldsymbol{r})$ is the local strain, and the spatially dependent elastic stiffness tensor $C_{ijkl}(\boldsymbol{r})$ can be written as a sum of homogeneous C_{ijkl}^0 and inhomogeneous part $C'_{ijkl}(\boldsymbol{r})$:

$$C_{ijkl}(\boldsymbol{r})=C_{ijkl}^0+C'_{ijkl}=C_{ijkl}^0+\left(\sum_p\eta_p^2(\boldsymbol{r},t)a_{ip}^pa_{jq}^pa_{kr}^pa_{ls}^pC_{pqrs}-C_{ijkl}^0\right) \tag{8}$$

where $\boldsymbol{a}$ is the transformation matrix representing the rotation of the coordinate system and is expressed in terms of the Euler angles φ_1, Φ and φ_2. The local stress is given as

$$\sigma_{ij}(\boldsymbol{r})=(C_{ijkl}^0+C'_{ijkl})(\bar{\varepsilon}_{kl}+\delta\varepsilon_{kl}(\boldsymbol{r})-\varepsilon_{kl}^0(\boldsymbol{r})) \tag{9}$$

where $\bar{\varepsilon}_{ij}$ and $\delta\varepsilon_{ij}(\boldsymbol{r})$ represent the homogeneous and heterogeneous strains, respectively, and $\varepsilon_{ij}^0(\boldsymbol{r})$ is the stress-free eigenstrain field that can arise from phase transformation. The heterogeneous strain is determined by the displacement as

$$\delta\varepsilon_{ij}(\boldsymbol{r})=\frac{1}{2}\left(\frac{\partial u_i(\boldsymbol{r})}{\partial r_j}+\frac{\partial u_j(\boldsymbol{r})}{\partial r_i}\right) \tag{10}$$

where $u_i(\boldsymbol{r})$ denotes the ith component of the displacement field. The local elastic field can be obtained by solving the mechanical equilibrium equation:

$$\frac{\partial \sigma_{ij}}{\partial r_j}=0 \tag{11}$$

From Eqs. (9), (10) and (11), we obtain:

$$C^0_{ijkl}\frac{\partial^2 u_k(\boldsymbol{r})}{\partial r_j \partial r_l}=\nabla_j\left\{\left[\sum_p \eta_p^2(\boldsymbol{r},t)a^p_{ip}a^p_{jq}a^p_{kr}a^p_{ls}C_{pqrs}\right]\cdot (\varepsilon^0_{ij}(\boldsymbol{r})-\bar{\varepsilon}_{ij})\right\}-\frac{\partial}{\partial r_j}\cdot \left\{\left[\sum_p \eta_p^2(\boldsymbol{r},t)a^p_{ip}a^p_{jq}a^p_{kr}a^p_{ls}C_{pqrs}-C^0_{ijkl}\right]\frac{\partial u_k(\boldsymbol{r})}{\partial r_l}\right\} \tag{12}$$

If we ignore the modulus and volume differences between the GBs and the interior and set $\varepsilon^0_{ij}(\boldsymbol{r})=0$ [42], Eq. (1) can be written as

$$\frac{\partial \eta_p(r,t)}{\partial t}=-L\{\frac{\partial mf(\eta_p)}{\delta \eta_p}+K_2\nabla^2\eta_p+ \eta_p a^p_{ip}a^p_{jq}a^p_{kr}a^p_{ls}C_{pqrs}[\delta\varepsilon_{ij}(\boldsymbol{r})\delta\varepsilon_{kl}(\boldsymbol{r})+ \bar{\varepsilon}_{ij}\bar{\varepsilon}_{kl}+2\delta\varepsilon_{ij}(\boldsymbol{r})\bar{\varepsilon}_{kl}]\} \tag{13}$$

According to the symmetry properties of the stiffness, the number of independent stiffness coefficients is reduced from 81 to 36, which means that the second-order and fourth-order symmetric tensors can be replaced by the relation 11→1; 22 → 2; 33→ 3; 23 or 32 →4; 31 or 13→ 5; 12 or 21→ 6. To assess the effects of Al, Y and Ca, the second-order symmetric tensors C_{ij} are calculated based on first principles calculations.

In this work, the stiffness coefficients and the GB energy in the alloy are the initial input parameters of the phase field model, and their values will be affected by the solutes. Therefore, first principles and MD calculations should be carried out first according to the solutes before the microstructure evolution simulation. The program flow chart of the simulation is shown in Fig. 1.

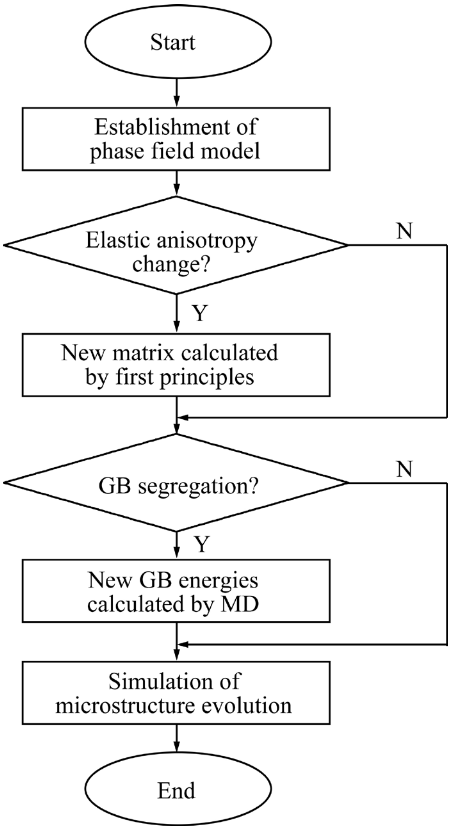

Fig. 1 Program flow chart of multiscale simulation for evolution of ZK60 alloy

2.2 First principles calculations

First-principles calculations were performed using the Vienna ab initio simulation package (VASP) [43,44] with Blochl's projector augmented wave (PAW) potential method [45]. The exchange-correlation energy functional was described with the generalized gradient approximation (GGA) as parameterized by Perdew−Burke−Ernzerhof (PBE) [46]. A 520 eV plane wave cutoff was adopted. The convergence criterion for energy and the atomic force were set as 10^{-6} eV and 10^{-2} eV/Å, respectively. Partial occupancies were determined by using the first-order Methfessel−Paxton method [47] with a smearing width of 0.2 eV. Relaxation of atomic coordinates and optimization of the shape and size of the model were adopted for all calculations. A Γ-centered k-point mesh of 18×18×10 was adopted for the HCP primitive cell and other supercells were scaled appropriately to keep the k-point density constant. To calculate different elastic constants, HCP cells containing 36 and 72 Mg atoms were constructed, in which the larger model is used as a supplementary calculation, and the calculation results prove that the influence of model size can be excluded. Then, one Mg atom was replaced with one Zn atom (2 Mg atoms were replaced with Zn in 72 atoms) for the ZK60 cell construction, and the position of the replacement atoms in the structure was random. Finally, different cells were obtained by replacing Mg atoms with different microalloyed atoms X one by one, as shown in Fig. 2. To better link atomic computation with macrostructure control, the elastic constants of alloys with different solute contents are calculated using the weight fraction as an independent variable in this work. After many calculations and data fitting, it can be found that the different occupations of solute atoms have little effect on the elastic constant, and the elastic constant shows a good linear relationship with the change in solute content at low solute concentrations. The stiffness matrix of different solutes can be obtained by data fitting, as shown in Fig. 3.

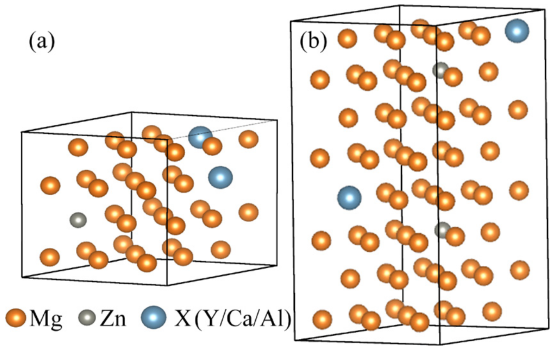

Fig. 2 Supercells used to model ZK60 alloying with Y, Ca or Al: (a) 36 atoms; (b) 72 atoms

Table 1 lists the elastic constants of alloys with 1 wt.% alloying elements. Since the maximum solid solubility of Al, Ca or Y in Mg alloys is greater than 1 wt.% [48], and the grains are considered a uniform solid solution in the microstructure evolution simulation, it is appropriate to consider the first principles calculation results as the approximate values of the elastic constants of ZK60 alloy after alloying.

2.3 Molecular dynamics simulations

To assess the effect of solute atom segregation on texture evolution in ZK60 alloy, the GB energy of different alloying atom segregation at the GB was estimated by the MD method and R−S model. The GBs segregated by solute atoms were simulated using relaxed bicrystal models in which the atoms segregated at the stable sites. The second nearest-neighbor modified embedded-atom method potentials of Mg−X (X=Ca, Al, Zn, and Y) binary systems were used in this work [49−51]. A stable low-angle TGB was obtained from the quenched MD simulation, in which the total energy of the system was minimized at 0 K by quenching the equilibrium system under the isothermal-isobaric

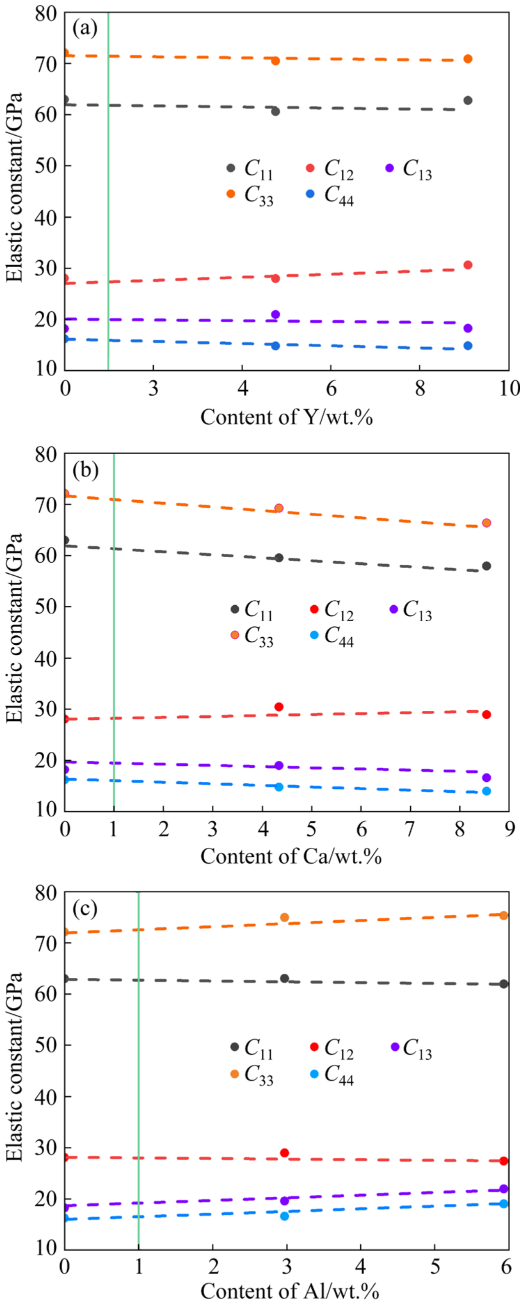

Fig. 3 Calculated elastic constants of ZK60 with different contents of alloying elements: (a) Y; (b) Ca; (c) Al

Table 1 Calculated elastic constants of ZK60 alloy with 1 wt.% alloying element

Alloy	C_{11}/GPa	C_{12}/GPa	C_{13}/GPa	C_{33}/GPa	C_{44}/GPa
Alloying with Y	62.12	27.40	20.75	69.86	17.36
Alloying with Ca	61.39	29.27	18.68	71.54	16.59
Alloying with Al	62.73	28.19	18.85	73.13	16.56
ZK60	62.96	28.15	18.21	72.10	16.24

ensemble at 50 K. The GB energies of ZK60 alloy with X addition were taken by measuring the energy in excess of that of a single crystal with the same number of X atoms distributed far away from each other. The results of Zn element segregation at the GB were taken as the GB energy of ZK60 alloy and were regarded as the benchmark to study the effect of segregation of other elements in ZK60 on GB properties in our simulation. The values of K_2^{ele} and m^{ele} were obtained from MD simulation and can be expressed as follows:

$$K_2^{\mathrm{ele}}(\theta)=E_K 10^{-12}\theta\frac{\pi}{180}\left[G_K-\ln\left(\theta\frac{\pi}{180}\right)\right] \tag{14a}$$

$$m^{\mathrm{ele}}(\theta)=E_m\theta\frac{\pi}{180}\left[G_m-\ln\left(\theta\frac{\pi}{180}\right)\right] \tag{14b}$$

By fitting the simulation results, when the values of E_K are 0.184, −0.396 and −0.285 while alloying with Y, Ca and Al, respectively, the corresponding values of E_m are 0.042, −0.09 and −0.065, and G_m=G_K=0.317. The relationship curve between the GB energy and dihedral angle is shown in Fig. 4.

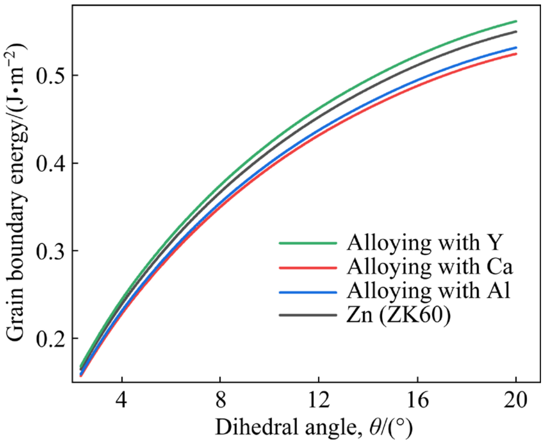

Fig. 4 GB energy of ZK60 alloy with different alloying elements segregated at GB based on R−S model

In this way, a 3D multiscale phase field model was proposed in which the model parameters of the elastic constants and grain boundary (GB) energy caused by the solutes were calculated from first principles and MD simulations. Other parameters were taken from our previous phase field simulations in ZK60 alloy [36]. The simulation was performed in a domain of 512×512×512 grid points and cyclic boundary conditions were adopted. To match the real microstructure in size, each grid point has a size of 0.3 μm. A unidirectional compressive stress of 270 MPa was taken to simulate a rolling process. A total of 100000 grains with arbitrary orientations defined by the Euler angle were adopted in our simulation system. A parallel computing message passing interface technique was utilized, and the time step t was taken as 0.5 s.

3 Results and discussion

3.1 Microstructure evolution

In our previous phase field simulations, we verified the influence of GB properties anisotropy on grain coarsening in ZK60 alloy. To verify the effect of elastic anisotropy on GB migration, we consider a bicrystal separated by a planar GB. The simulation cell is shown in Fig. 5. The grains are oriented at 0° and 30°, 0° and 45°, respectively, with respect to a fixed reference frame. The simulation cell is assumed to be periodic along all three directions and then subjected to uniaxial applied strain, ε_{zz}=0.01, while other axes are assumed to be free. The difference between the stored elastic energy densities between the two grains provides the driving force for GB migration; otherwise, the GB will remain static. In an elastic anisotropic system, the driving force (ΔF) can be calculated by [42]

$$\Delta F=E_{\mathrm{e}}^{1}-E_{\mathrm{e}}^{2} \tag{15}$$

where E_{e}^{1} and E_{e}^{2} represent the elastic energy densities in Grains 1 and 2, respectively. The GB velocity (v) is 8×10^{-4} in nondimensional units when the misorientation is 30° and 1.28×10^{-3} when the misorientation is 45°. In most studies of GB migration, it is assumed that the velocity of the GB

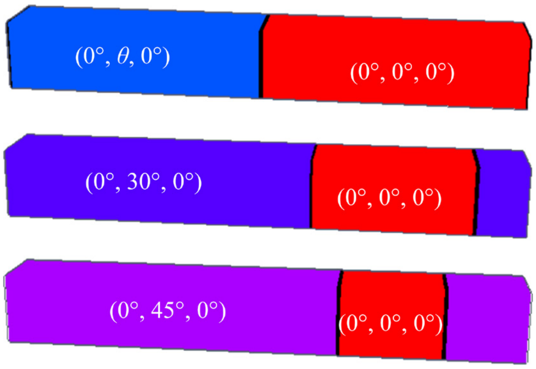

Fig. 5 GB motion in bicrystal with misorientation of 30° and 45°

is proportional to the driving force and can be obtained by $v=M\Delta F$, where M is the GB mobility and is expected to be a function of temperature. We use this relationship to verify the GB movement. In the simulation, the ratio of the driving force ($\Delta F_{30°}/\Delta F_{45°}$) is found to be 1.601, which is consistent with the ratio of the GB velocity ($v_{30°}/v_{45°}$=1.600).

Based on the principle of energy minimization, grains with lower elastic energy density grow at the expense of grains with higher elastic energy density and the boundary moves toward the grain oriented at 0°. Next, a series of calculations can be used to analyze GB migration [52], and the stored elastic energy density is $E_e=1/2\sigma_{ij}\varepsilon_{ij}$. For the case of a linear elastic crystal with the grain oriented at 0°, the free energy is

$$E_e=\frac{1}{2}\left[\frac{-C_{13}^2}{C_{11}+C_{12}}+\frac{-C_{23}^2}{C_{22}+C_{12}}+C_{33}\right]\varepsilon^2 \qquad (16)$$

The elastic energy in the grain rotated by θ can also be calculated with the elastic constant after rotation. From Eq. (15), we obtain the ratio of the driving force to be 1.58. Thus, we get good agreement between the driving force obtained from analysis and that obtained from the simulation.

We define the grains whose orientation difference (angle difference) is less than 1% from the normal direction of the base plane as the grains that constitute the basal texture. In Fig. 6, it can be seen that grains coarsen significantly, and the level

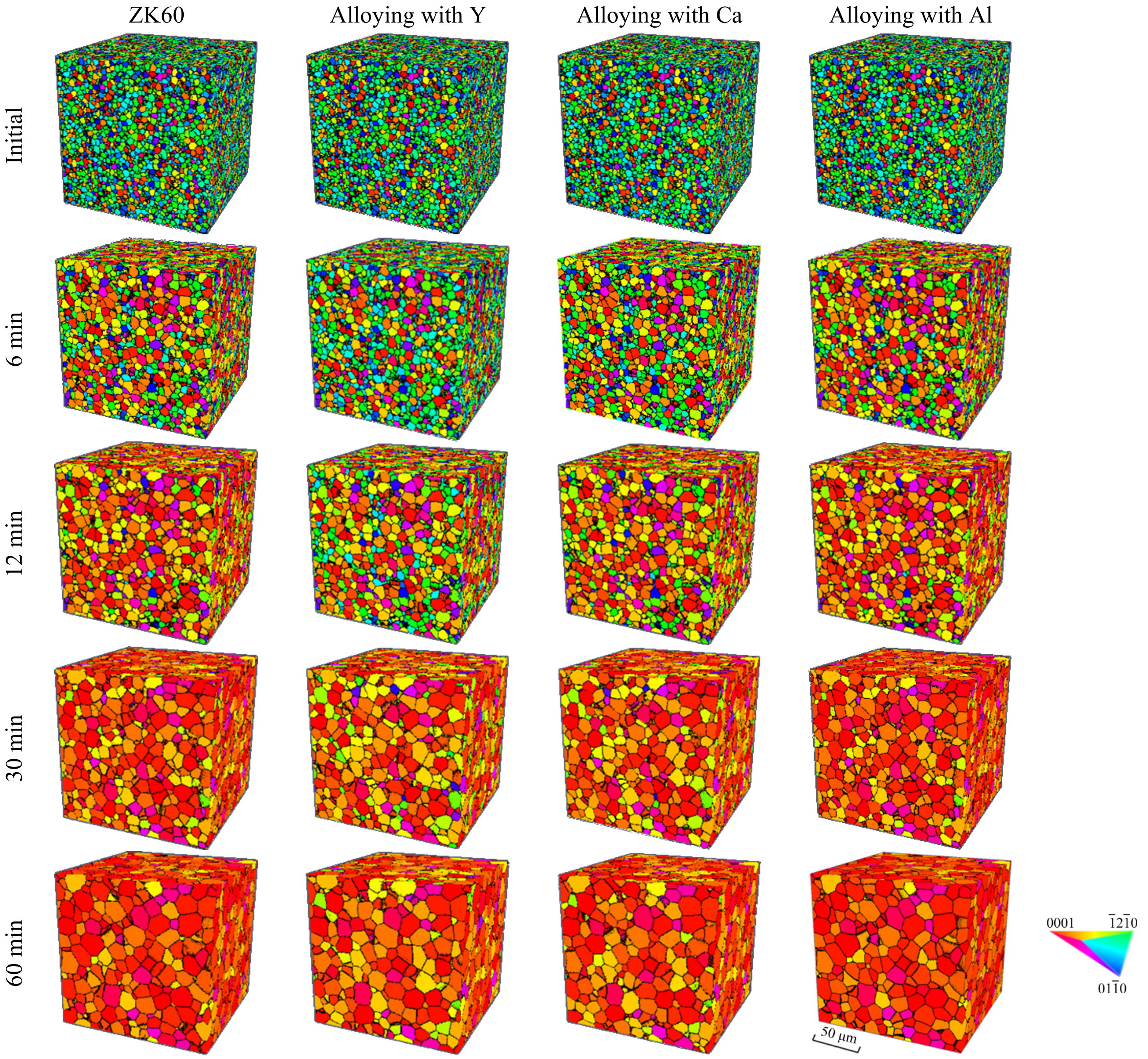

Fig. 6 Microstructure evolution with time at 573 K for ZK60 alloy containing different alloying elements under compression stress of 270 MPa

of the basal texture also increases with time, which means that grains with different orientations have varied driving forces during the coarsening process. A more severe basal texture is formed in ZK60 alloy with Al added after 6 min; in contrast, the basal texture level of ZK60 alloy containing Y or Ca is weaker at the same time. In the ZK60 alloy containing Y, even after 12 min, the microstructure still shows obvious random orientations. The dynamics data in all the systems were analyzed for a further quantitative comparison. The content of basal texture in the ZK60 alloy containing different alloying elements is shown in Fig. 7. It can be found that alloying with Al increases the level of basal texture; in contrast, alloying with Y or Ca shows an opposite effect, which well reproduces the previous experimental results [9−11,13,40]. Quantitatively speaking, the addition of 1 wt.% Y decreases the basal texture by 3.7% less than that of Ca and 5.6% less than that of ZK60 alloy when annealed at 573 K for 60 min, while the addition of 1 wt.% Al contributes a 1.3% increase in the basal texture in ZK60. It can be concluded that the addition of alloying elements changes the strength of the basal texture in ZK60 alloy coarsening under applied compression stress, which means that the elastic anisotropy is an important factor affecting the texture of the ZK60 alloy.

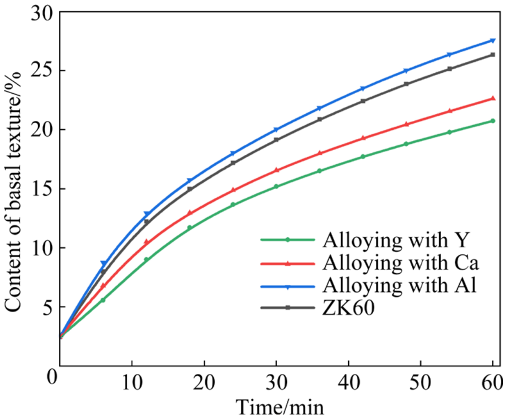

Fig. 7 Basal texture evolution in ZK60 containing different alloying elements at 573 K under compression stress of 270 MPa

3.2 Analysis of morphological topology

Quantitative topological analysis was carried out to further study the microstructure features. The grain size distributions are normalized with the mean grain size (R_{cr}). Apparently, the initial grain size distribution matches well with the Hillert distribution, as shown in Fig. 8, since it is chosen in a steady state during normal grain growth [53,54]. The frequency of the grain size distribution increases gradually until it reaches the maximum at 8/9 of the average grain size and then decreases rapidly. The area between the different grain size

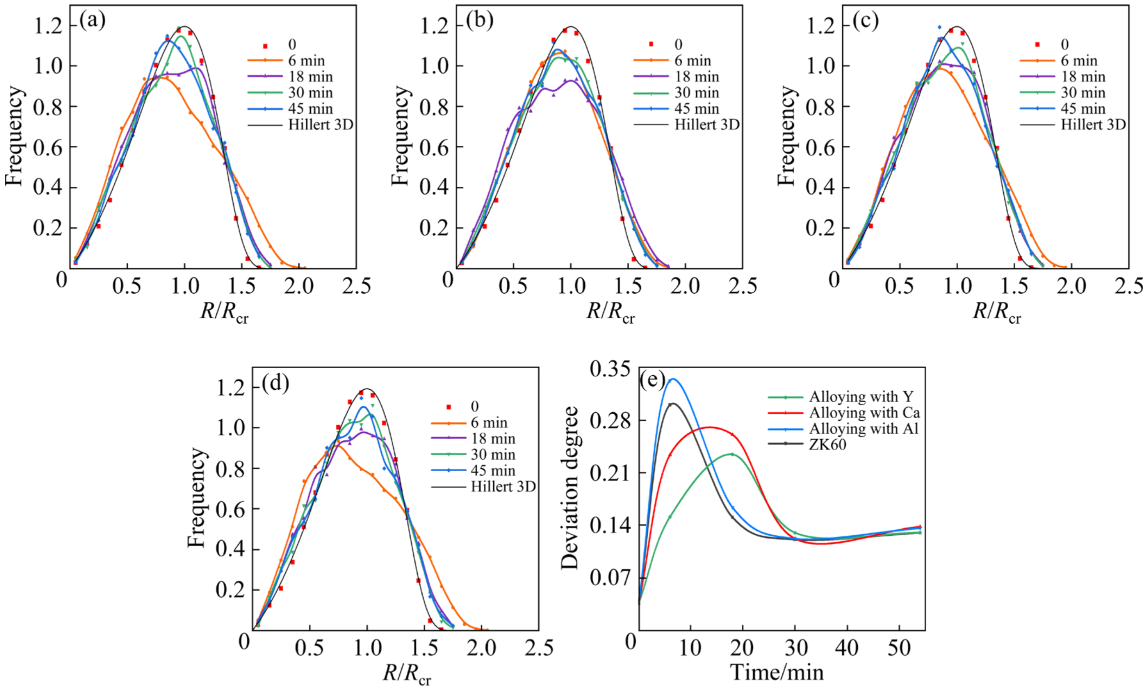

Fig. 8 Grain distributions of ZK60 alloy with different alloying elements at different annealing time under stress: (a) ZK60; (b) Alloying with Y; (c) Alloying with Ca; (d) Alloying with Al; (e) Deviation degree

distribution curves and the Hillert 3D model was calculated to characterize the deviation between the real grain size distribution and the Hillert distribution. The distribution deviates from the Hillert distribution once the stress field is applied, and after a period of grain coarsening, the distribution curves start moving closer to the Hillert distribution again. The maximum grain size is over $2R_{\text{cr}}$, which means that the microstructure is no longer the result of a steady-state normal grain growth. The distribution deviation may be caused by abnormal grain growth, and according to Hillert's research [55], some grains are much larger than average. According to the deviation level curve shown in Fig. 8(e), Ca or Y reduces the deviation of the grain distribution curve, which means that the abnormal growth degree is reduced, while Al is the opposite case.

The grain size fluctuation can be expressed as $\Delta d=(d_{\max}-d_{\min})/d_{\text{average}}$ [31]. The values of $d_{\max}$ and $d_{\min}$ represent the average size of the first 5% and the last 5% of the grains in the row from large to small volume, respectively. The grain size fluctuation in Fig. 9 shows an obvious rise when the compression stress is applied and then falls gradually after 20−30 min, which agrees well with the grain size distribution deviation above and confirms that some grains grow abnormally at this stage. The change in orientation distribution during grain growth under stress contributes to the increase in fluctuation. The growth driving force of a grain in the absence of an applied load depends on its curvature, which is determined by the grain and its surrounding grains. However, under an applied compression stress, the elastic anisotropy plays a more important role, and the growth rate of each grain is determined by the orientation difference between the grain and its adjacent grains. The grains with orientations close to ⟨0001⟩ show greater growth speeds, as shown in Fig. 6, and the grains with orientations away from ⟨0001⟩ promote the abnormal growth for basal oriented grains during coarsening.

In contrast to Al, there is a significant decrease in the peak value of the grain size fluctuation curve when alloying with Ca or Y in ZK60 alloy. Apparently, this can be attributed to the reduction of the elastic energy difference between grains with different orientations after the addition of Ca or Y. The decrease in the elastic energy difference reduces the difference in the grain growth rate at the stage of abnormal grain growth, which finally results in a more homogeneous microstructure with time. The grain size distribution and fluctuation are not back to the initial situation in the end. This may be mainly caused by two reasons: one is that the elastic energy differences between grains with different orientations are still at a high level for polycrystalline evolution, and the other is that the anisotropy of GB properties is adopted in our model, which is not considered in Hillert's model.

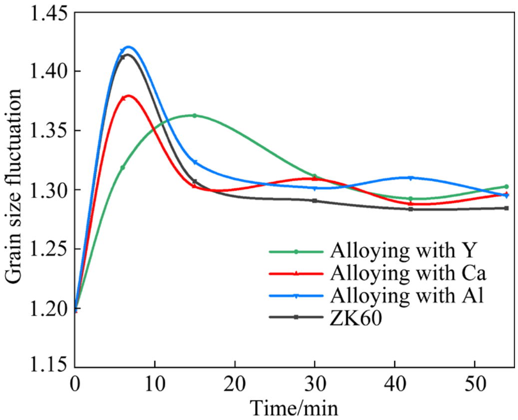

Fig. 9 Grain size fluctuation of ZK60 alloy with different alloying elements at 573 K under compression stress of 270 MPa

3.3 Effect of grain boundary energy on texture evolution

In addition to the contribution of elastic anisotropy influenced by alloying elements, some researchers have speculated that solute segregation at GBs may be one of the important factors weakening the texture in Mg alloys [56,57]. Solute atoms in the polycrystalline tend to segregate at GBs, which results in a change in GB energy, as shown in Fig. 4. Obviously, the GB energy decrease caused by Ca or Al segregation at the GB is greater than that caused by Zn segregation; in contrast, it shows a higher GB energy when Y segregates. The variation in GB energy is mainly affected by the atomic radius difference according to MD simulations, which can be explained by the elastic interaction between atoms. GB with lower GB energy is more stable, which also makes GB migration harder. The microstructure in ZK60 alloy with different alloying elements segregating at the GBs is shown in Fig. 10. The difference in texture in different cases is small, so a quantitative analysis was carried out by drawing the content change

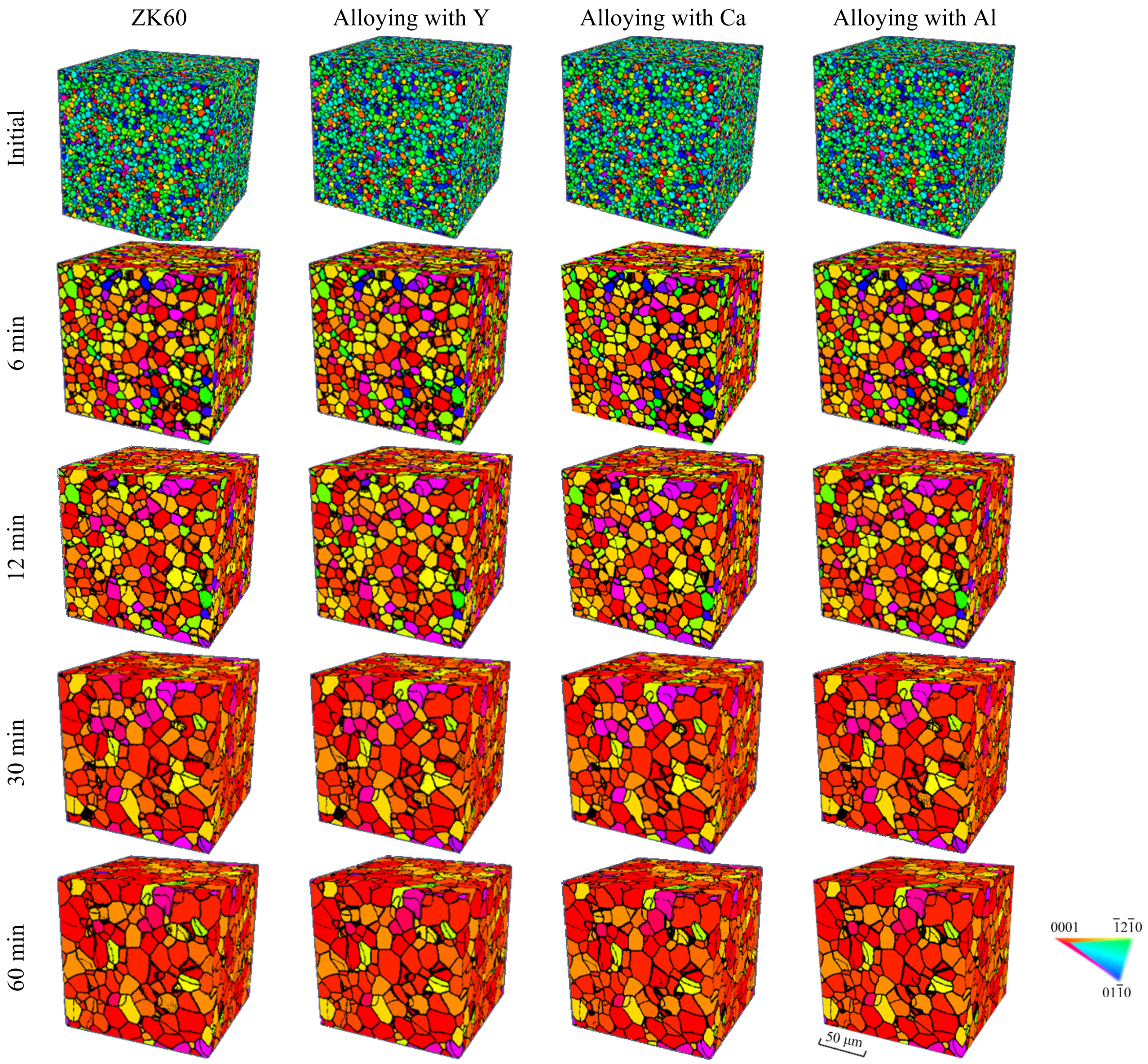

Fig. 10 Microstructure evolution with time at 573 K in ZK60 alloy with different alloying elements segregated at GBs under compression stress of 270 MPa

curve of ⟨0001⟩-oriented grains, as shown in Fig. 11. The change rate of the basal texture strength compared to ZK60 was calculated as $(C-C_{\mathrm{ZK60}})/C_{\mathrm{ZK60}}$. As predicted, with the decrease in the GB energy caused by solute atoms, the strength of the basal texture decreases, and Ca shows the best texture weakening effect in ZK60 alloy. However, the addition of Y cannot weaken the texture. The simulation results show that the segregation of some solute atoms will indeed play a role in the microstructure evolution of ZK60 alloy; however, compared with the effect of elastic anisotropy change, the effect of GB energy change caused by segregation on the microstructure evolution is too small (less than 1%). In summary, when considering the effects of both elastic anisotropy and GB segregation on texture, the addition of Ca or Y in the ZK60 alloy can suppress the basal texture and thus improve the formability.

The effect of the average behavior of alloying atoms at the micro level on the macrotexture of ZK60 alloy was primarily investigated in this study. To balance calculation efficiency and accuracy, it was assumed that the polycrystals in the model were homogeneous solid solutions. Furthermore, a simplified model was employed in which essential parameters were transferred between simulations at different scales. In future work, the atomic simulation method can be used to establish a dynamic database containing various types of GBs,

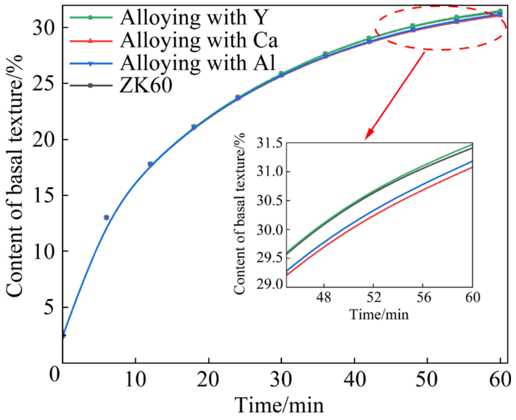

Fig. 11 Content of basal texture during microstructure evolution in ZK60 alloy with different alloying elements at 270 MPa and 573 K

and the diffusion behavior of solute atoms near the interface can be simulated through adaptive grid division. In addition, the automation and calculation efficiency can be further improved by establishing an appropriate atomic scale simulation call modules under the framework of phase field simulation.

4 Conclusions

(1) Ca and Y can weaken the basal texture (by 3.7%−5.6%), while Al exhibits the opposite effect.

(2) The elastic anisotropy leads to abnormal grain growth and the distribution of grain size deviates from the Hillert distribution, in which Ca or Y reduces the deviation of the distribution curve with a smaller grain size fluctuation, while Al has the opposite case.

(3) In GB segregation cases, the segregation of Ca or Al atoms weakens the texture, while Y does not. The change caused by GB segregation is weak (less than 1%) compared with the elastic anisotropy.

CRediT authorship contribution statement

Yu-hao SONG: Conceptualization, Methodology, Software, Investigation, Formal analysis, Writing − Original draft; **Ming-tao WANG:** Methodology, Resources, Wring − Review & editing; **Jun-yuan BAI:** Investigation, Formal analysis; **Jian-feng JIN:** Software; **Pei-jun YANG:** Investigation; **Ya-ping ZONG:** Methodology; **Gao-wu QIN:** Wring − Review & editing.

Declaration of competing interest

The authors declare that they have no known competing financial interests or person relationships that could have appeared to influence the work reported in this paper.

Acknowledgments

The authors would like to acknowledge the financial support of the “111” Project, China (No. B20029), and the Fundamental Research Funds for the Central Universities, China (Nos. N2002017, N2007011).

References

[1] FAKHAR N, SABBAGHIAN M. Hot shear deformation constitutive analysis of fine-grained ZK60 Mg alloy sheet fabricated via dual equal channel lateral extrusion and sheet extrusion [J]. Transactions of Nonferrous Metals Society of China, 2022, 32(8): 2541−2556.

[2] JIANG Bin, DONG Zhi-hua, ZHANG Ang, SONG Jiang-feng, PAN Fu-sheng. Recent advances in micro-alloyed wrought magnesium alloys: Theory and design [J]. Transactions of Nonferrous Metals Society of China, 2022, 32(6): 1741−1780.

[3] CHEN Zhen-hua. Magnesium alloy [M]. Beijing: Chemical Industry Press, 2004: 477. (in Chinese)

[4] MILLER V M, BERMAN T D, BEYERLEIN I J, JONES J W, POLLOCK T M. Prediction of the plastic anisotropy of magnesium alloys with synthetic textures and implications for the effect of texture on formability [J]. Materials Science and Engineering A, 2016, 675: 345−360.

[5] DU Yu-zhou, LIU Dong-jie, GE Yan-feng, JIANG Bai-ling. Effects of deformation parameters on microstructure and texture of Mg−Zn−Ce alloy [J]. Transactions of Nonferrous Metals Society of China, 2020, 30(10): 2658−2668.

[6] WANG Wen-ke, MA Li-min, CHAI Shao-chun, ZHANG Wen-cong, CHEN Wen-zhen, FENG Yang-ju, CUI Guo-rong. Role of one direction strong texture in stretch formability for ZK60 magnesium alloy sheet [J]. Materials Science and Engineering A, 2018, 730: 162−167.

[7] GONG Xi-bin, KANG S B, LI Sai-yi, CHO J H. Enhanced plasticity of twin-roll cast ZK60 magnesium alloy through differential speed rolling [J]. Materials & Design, 2009, 30: 3345−3350.

[8] WANG Wen-ke, ZHANG Wen-cong, CHEN Wen-zhen, CUI Guo-rong, WANG Er-de. Effect of initial texture on the bending behavior, microstructure and texture evolution of ZK60 magnesium alloy during the bending process [J]. Journal of Alloys and Compounds, 2018, 737: 505−514.

[9] LI Xiao-yan, LI Xing-lin, GUO Fei, JIANG Lu-yao, HU Hong-jun, YAN Ming-bo. Research progress on recrystallization texture and its modification of magnesium alloys [J]. Transactions of Materials and Heat Treatment, 2020, 41(9): 17−29. (in Chinese)

[10] GUO Fei. Deformation behavior of large strain rolling of Mg alloys sheets and its effect on microstructures and properties [D]. Chongqing: Chongqing University, 2017: 106. (in Chinese)

[11] FARZADFAR S A, SANJARI M, JUNG I H, ESSADIQI E,

YUE S. Role of yttrium in the microstructure and texture evolution of Mg [J]. Materials Science and Engineering A, 2011, 528: 6742−6753.

[12] JUNG I H, SANJARI M, KIM J, YUE S. Role of RE in the deformation and recrystallization of Mg alloy and a new alloy design concept for Mg−RE alloys [J]. Scripta Materialia, 2015, 102: 1−6.

[13] DING Han-lin, SHI Xiao-bin, WANG Yong-qiang, CHENG Guang-ping, KAMADO S. Texture weakening and ductility variation of Mg−2Zn alloy with CA or RE addition [J]. Materials Science and Engineering A, 2015, 645: 196−204.

[14] WANG Hui-yuan, XIA Nan, BU Ru-yu, WANG Cheng, ZHA Min, YANG Zhi-zheng. Current research and future prospect on low-alloyed high-performance wrought magnesium alloys [J]. Acta Metallurgica Sinica, 2021, 57(11): 1429−1437. (in Chinese)

[15] LIU Chun-quan, CHEN Xian-hua, CHEN Jiao, ZHAO Chao-yue, DAI Yan, LIU Xiao-feng, ZHAO Di, LUO Zhu, TU Teng, PAN Fu-sheng. Effect of calcium on microstructure, texture and mechanical properties of Mg−4Zn alloy [J]. Rare Metal Materials and Engineering, 2019, 48(11): 3506−3513.

[16] ZHAO Hong-liang, HUA Yun-xiao, DONG Xiang-lei, XING Hui, LU Yan-li. Influence of trace Ca addition on texture and stretch formability of AM50 magnesium alloy sheet [J]. Transactions of Nonferrous Metals Society of China, 2020, 30(3): 647−656.

[17] DING Han-lin, ZHANG Peng, CHENG Guang-ping, KAMADO S. Effect of calcium addition on microstructure and texture modification of Mg rolled sheets [J]. Transactions of Nonferrous Metals Society of China, 2015, 25(9): 2875−2883.

[18] KIM D U, CHA P R, KIM S G, KIM W T, CHO J, HAN H N, LEE H J, KIM J. Effect of micro-elasticity on grain growth and texture evolution: A phase field grain growth simulation [J]. Computational Materials Science, 2012, 56: 58−68.

[19] LIU Q K K, SCHUMACHER G. Texture evolution during crystallization of thin amorphous films [J]. MRS Proceedings, 2002, 749: W12.2.

[20] MURRAY C E, TREGER M, NOYAN I C, ROSENBERG R. Evolution of strain energy during recrystallization of plated Cu films [J]. IEEE Transactions on Device & Materials Reliability, 2016, 16(4): 440−445.

[21] SONNWEBERRIBIC P, GRUBER P, DEHM G, ARZT E. Texture transition in Cu thin films: Electron backscatter diffraction vs. X-ray diffraction [J]. Acta Materialia, 2006, 54: 3863−3870.

[22] LEE S B, KIM D I, HONG S H, LEE D N. Texture evolution of abnormal grains with post-deposition annealing temperature in nanocrystalline Cu thin films [J]. Metallurgical and Materials Transactions A, 2012, 44(1): 152−162.

[23] XIN T, ZHAO Yu-hong, MAHJOUB R, JIANG Jia-xi, YADAV A, NOMOTO K, NIU R, TANG Song, JI Fan, QUADIR Z, MISKOVIC D, DANIELS J, XU W, LIAO X, CHEN Long-qing, HAGIHARA K, LI Xiao-yan, RINGER S, FERRY M. Ultrahigh specific strength in a magnesium alloy strengthened by spinodal decomposition [J]. Science Advances, 2021, 7(23): 1−9.

[24] TIAN Xiao-lin, ZHAO Yu-hong, PENG Dun-wei, GUO Qing-wei, GUO Zhen, HOU Hua. Phase-field crystal simulation of evolution of liquid pools in grain boundary pre-melting regions [J]. Transactions of Nonferrous Metals Society of China, 2021, 31(4): 1175−1188.

[25] CHEN Long-qing, ZHAO Yu-hong. From classical thermodynamics to phase-field method [J]. Progress in Materials Science, 2021, 124: 100868.

[26] ZHAO Yu-hong, LIU Ke-xin, HOU Hua, CHEN Long-qing. Role of interfacial energy anisotropy in dendrite orientation in Al−Zn alloys: A phase field study [J]. Materials & Design, 2022, 216: 110555.

[27] XIN T, TANG Song, JI Fan, CUI L, HE Bin-bin, LIN Xin, TIAN Xiao-lin, HOU Hua, ZHAO Yu-hong, FERRY M. Phase transformations in an ultralight BCC Mg alloy during anisothermal ageing [J]. Acta Materialia, 2022, 239: 118248.

[28] CHEN L, CHEN J, LEBENSOHN R A, JI Y Z, HEO T W, BHATTACHARYYA S, CHANG K, MATHAUDHU S, LIU Z K, CHEN L Q. An integrated fast Fourier transform-based phase-field and crystal plasticity approach to model recrystallization of three dimensional polycrystals [J]. Computer Methods in Applied Mechanics and Engineering, 2015, 285: 829−848.

[29] HU Xin, JI Y, HEO T W, CHEN Long-qing, CUI Xiang-yang. Phase-field model of deformation twin-grain boundary interactions in hexagonal systems [J]. Acta Materialia, 2020, 200: 821−834.

[30] LI Y, HU S, BARKER E, OVERMAN N, WHALEN S, MATHAUDHU S. Effect of grain structure and strain rate on dynamic recrystallization and deformation behavior: A phase field-crystal plasticity model [J]. Computational Materials Science, 2020, 180: 109707.

[31] SONG Yu-hao, WANG Ming-tao, NI Jia, JIN Jian-feng, ZONG Ya-ping. Effect of grain boundary energy anisotropy on grain growth in ZK60 alloy using a 3D phase-field modeling [J]. Chinese Physics B, 2020, 29(12): 128201.

[32] MIYOSHI E, TAKAKI T. Multi-phase-field study of the effects of anisotropic grain-boundary properties on polycrystalline grain growth [J]. Journal of Crystal Growth, 2017, 474: 160−165.

[33] SUWA Y, SAITO Y, ONODERA H. Three-dimensional phase field simulation of the effect of anisotropy in grain-boundary mobility on growth kinetics and morphology of grain structure [J]. Computational Materials Science, 2007, 40(1): 40−50.

[34] SHAHNOOSHI E, JAMSHIDIAN M, JAFARI M, ZIAEI-RAD S, RABCZUK T. Phase field modeling of stressed grain growth: Effect of inclination and misorientation dependence of grain boundary energy [J]. Journal of Crystal Growth, 2019, 518: 18−29.

[35] ALLEN S M, CAHN J W. A microscopic theory for antiphase boundary motion and its application to antiphase domain coarsening [J]. Acta Metallurgica, 1979, 27: 1085−1095.

[36] SONG Yu-hao, WANG Ming-tao, ZONG Ya-ping, HE Ri, JIN Jian-feng. Grain refinement by second phase particles under applied stress in ZK60 Mg alloy with Y through phase field simulation [J]. Materials (Basel), 2018, 11(10): 1903.

[37] VEDANTAM S, PATNAIK B S. Efficient numerical algorithm for multiphase field simulations [J]. Physical Review E, 2006, 73: 016703.

[38] CHANG K, CHEN Long-qing, KRILL C E, MOELANS N. Effect of strong nonuniformity in grain boundary energy on 3-D grain growth behavior: A phase-field simulation study [J]. Computational Materials Science, 2017, 127: 67−77.

[39] DING Han-lin, WANG Tian-yi, XU Cheng-zhi, LI Dian-kai. Effects of Ca addition and deformation conditions on microstructure and texture of Mg−Zn alloy [J]. The Chinese Journal of Nonferrous Metals, 2015, 25: 1142−1152. (in Chinese)

[40] BOHLEN J, NÜRNBERG M R, SENN J W, LETZIG D, AGNEW S R. The texture and anisotropy of magnesium–zinc−rare earth alloy sheets [J]. Acta Materialia, 2007, 55: 2101−2112.

[41] KHACHATURYAN A G. Theory of structural transformations in solids [M]. New York: Dover Publications, 1983.

[42] BHATTACHARYYA S, HEO T W, CHANG K, CHEN Long-qing. A phase-field model of stress effect on grain boundary migration [J]. Modelling and Simulation in Materials Science and Engineering, 2011, 19(3): 035002.

[43] KRESSE G, HAFNER J. Ab initio molecular dynamics for liquid metals [J]. Journal of Non-Crystalline Solids, 1993, 47(1): 558−561.

[44] KRESSE G, HAFNER J. Ab initio molecular dynamics for open-shell transition metals [J]. Physical Review B, 1993, 48(17): 13115−13118.

[45] BLOCHL P E. Projector augmented-wave method [J]. Physical Review B, 1994, 50(24): 17953−17979.

[46] PERDEW J P, BURKE K, ERNZERHOF M. Generalized gradient approximation made simple [J]. Physical Review Letters, 1996, 77(18): 3865−3866.

[47] METHFESSEL M, PAXTON A T. High-precision sampling for Brillouin-zone integration in metals [J]. Physical Review B, 1989, 40(6): 3616−3621.

[48] TANG Ren-zheng, TIAN Rong-zhang. Binary alloy phase diagrams and crystal structure of intermediate phase [M]. Changsha: Central South University Press, 2009. (in Chinese)

[49] KIM Y M, KIM N J, LEE B J. Atomistic modeling of pure Mg and Mg−Al systems [J]. Calphad, 2009, 33: 650−657.

[50] KIM K H, JEON J B, LEE B J. Modified embedded-atom method interatomic potentials for Mg–X (X=Y, Sn, Ca) binary systems [J]. Calphad, 2015, 48: 27−34.

[51] JANG H S, KIM K M, LEE B J. Modified embedded-atom method interatomic potentials for pure Zn and Mg−Zn binary system [J]. Calphad, 2018, 60: 200−207.

[52] ZHANG H, MENDELEV M I, SROLOVITZ D J. Computer simulation of the elastically driven migration of a flat grain boundary [J]. Acta Materialia, 2004, 52: 2569−2576.

[53] YADAV V, MOELANS N. Analysis of grain topology and volumetric growth rate relation in three-dimensional normal grain growth [J]. Acta Materialia, 2018, 156: 275−286.

[54] YADAV V, MOELANS N. Investigation on the existence of a ‘Hillert regime’ in normal grain growth [J]. Scripta Materialia, 2018, 142: 148−152.

[55] HILLERT M. On the theory of normal and abnormal grain growth [J]. Acta Materialia, 1965, 13: 227−238.

[56] WANG Qing-hang, JIANG Bin, TANG Ai-tao, FU Jie, JIANG Zhong-tao, SHENG Hao-ran, ZHANG Ding-fei, HUANG Guang-sheng , PAN Fu-sheng. Unveiling annealing texture formation and static recrystallization kinetics of hot-rolled Mg−Al−Zn−Mn−Ca alloy [J]. Journal of Materials Science & Technology, 2020, 43: 104−118.

[57] STANFORD N, SHA G, XIA J H, RINGER S P, BARNETT M R. Solute segregation and texture modification in an extruded magnesium alloy containing gadolinium [J]. Scripta Materialia, 2011, 65: 919−921.

相场法模拟溶质对 ZK60 合金晶粒长大过程中织构演化的影响

宋宇豪，王明涛，白俊源，金剑锋，杨培军，宗亚平，秦高梧

东北大学 材料科学与工程学院 材料各向异性与织构教育部重点实验室，沈阳 110819

摘　要：建立包含受溶质影响的弹性各向异性及晶界偏析的多尺度三维相场模型，研究溶质原子 Ca、Y 和 Al 对 ZK60 合金在 270 MPa 压应力及 573 K 下晶粒生长过程中织构演变的影响。结果表明，添加 Ca 或 Y 均可以弱化 ZK60 的基面织构，而添加 Al 则会增强织构。添加 Al 后，晶粒尺寸分布与 Hillert 模型之间的偏差增大，而添加 Ca 或 Y 会使偏差减小。与弹性各向异性相比，溶质偏析引起的晶界能变化对织构演化的影响十分有限。揭示的机理对在 ZK60 合金显微组织设计中采用合适的合金化策略具有重要意义。

关键词：相场模型；弹性各向异性；溶质偏析；织构演化；ZK60 合金；合金化

(Edited by Bing YANG)